








RESEARCH ARTICLE | JANUARY 23 2025

Thermalization of a flexible microwave stripline measured by a superconducting qubit

Patrick Paluch ; Martin Spiecker ; Nicolas Gosling ; Viktor Adam ; Jakob Kammhuber; Kiefer Vermeulen ; Daniël Bouman ; Wolfgang Wernsdorfer ; Ioan M. Pop  

 Check for updates

Appl. Phys. Lett. 126, 034003 (2025)

<https://doi.org/10.1063/5.0243116>



View Online



Export Citation

Articles You May Be Interested In

Tunable coupling scheme for implementing two-qubit gates on fluxonium qubits

Appl. Phys. Lett. (November 2021)

Operating in a deep underground facility improves the locking of gradiometric fluxonium qubits at the sweet spots

Appl. Phys. Lett. (February 2022)

Equivalence of flexible stripline and coaxial cables for superconducting qubit control and readout pulses

Appl. Phys. Lett. (May 2024)



Applied Physics Letters

Special Topics Open for Submissions

[Learn More](#)

Thermalization of a flexible microwave stripline measured by a superconducting qubit

Cite as: Appl. Phys. Lett. **126**, 034003 (2025); doi: [10.1063/5.0243116](https://doi.org/10.1063/5.0243116)

Submitted: 9 October 2024 · Accepted: 11 January 2025 ·

Published Online: 23 January 2025



View Online



Export Citation



CrossMark

Patrick Paluch,^{1,2}  Martin Spiecker,^{1,2}  Nicolas Gosling,^{1,2}  Viktor Adam,^{1,2}  Jakob Kammhuber,³
Kiefer Vermeulen,³  Daniël Bouman,³  Wolfgang Wernsdorfer,^{1,2}  and Ioan M. Pop^{1,2,4,a)} 

AFFILIATIONS

¹IQMT, Karlsruhe Institute of Technology, 76131 Karlsruhe, Germany

²PHI, Karlsruhe Institute of Technology, 76131 Karlsruhe, Germany

³Delft Circuits B.V., Lorentzweg 1, 2628CJ Delft, The Netherlands

⁴PII, Stuttgart University, 70569 Stuttgart, Germany

^{a)} Author to whom correspondence should be addressed: ioan.pop@kit.edu

ABSTRACT

With the demand for scalable cryogenic microwave circuitry continuously rising, recently developed flexible microwave striplines offer the tantalizing perspective of increasing the cabling density by an order of magnitude without thermally overloading the cryostat. We use a superconducting quantum circuit to test the thermalization of input flex cables with integrated 60 dB of attenuation distributed at various temperature stages. From the measured decoherence rate of a superconducting fluxonium qubit, we estimate a residual population of the readout resonator of $(2.2 \pm 0.9) \times 10^{-3}$ photons and we measure a 0.28 ms thermalization time for the flexible stripline attenuators. Furthermore, we confirm that the qubit reaches an effective temperature of 26.4 mK, close to the base temperature of the cryostat, practically the same as when using a conventional semi-rigid coaxial cable setup.

© 2025 Author(s). All article content, except where otherwise noted, is licensed under a Creative Commons Attribution (CC BY) license (<https://creativecommons.org/licenses/by/4.0/>). <https://doi.org/10.1063/5.0243116>

The growing size of cryogenic quantum processors^{1–5} and detector arrays^{6–9} requires an increasing microwave circuitry density for readout and control. Possible strategies to cope with this challenge consist in frequency or time-division multiplexing,^{10–14} which are, however, limited by the available bandwidth and the finite lifetime of the measured states. This motivates the demand for increasingly denser cryogenic microwave circuitry compatible with high-coherence devices,¹⁵ for which new platforms based on photonic links^{16–18} or flexible microwave striplines^{19–25} have recently been developed.

Flexible striplines with integrated microwave attenuators and filters promise to increase the cabling density by at least one order of magnitude compared to conventional coaxial setups. Here, we use a superconducting fluxonium qubit in a circuit quantum electrodynamics (QED) readout architecture to measure their *in situ* thermalization time and contribution to photon shot noise dephasing. We show that the flexible stripline thermalizes with a time constant of 0.28 ms, almost a factor of two faster than cryogenic coaxial attenuators in a similar setup, and we measure residual photon populations of $(2.2 \pm 0.9) \times 10^{-3}$. These findings, combined with the fact that we do not observe any detrimental effects on the superconducting device,

encourage the use of flexible striplines at scale in future quantum processor setups and large detector arrays.

In the last two decades, superconducting qubits have emerged as one of the most promising candidates for future large-scale quantum processors.^{1–5} One reason for this development is the steadily increasing qubit coherence time, nowadays exceeding a few hundred microseconds.^{28–30} This improvement also results in a higher sensitivity to dephasing, a measure for fluctuations of the qubit frequency, that originates from a multitude of different noise sources.^{31–33} The standard tool to read out quantum information in circuit QED is the dispersive coupling of the qubit to a readout resonator or cavity,³⁴ which, however, adds another noise source for dephasing. This so-called photon shot noise arises from the fact that each photon in the resonator changes the qubit frequency by the dispersive shift $\chi/2\pi$.^{35–38} In this way, fluctuations in the average resonator photon number \bar{n} directly translate into qubit dephasing.

Excess photons in the resonator originate from heat loaded in attenuators or filters anchored at higher temperature stages, transmitted via the microwave lines in form of blackbody radiation³⁹ [Fig. 1(a)]. In experiments with resonators in the gigahertz (GHz)

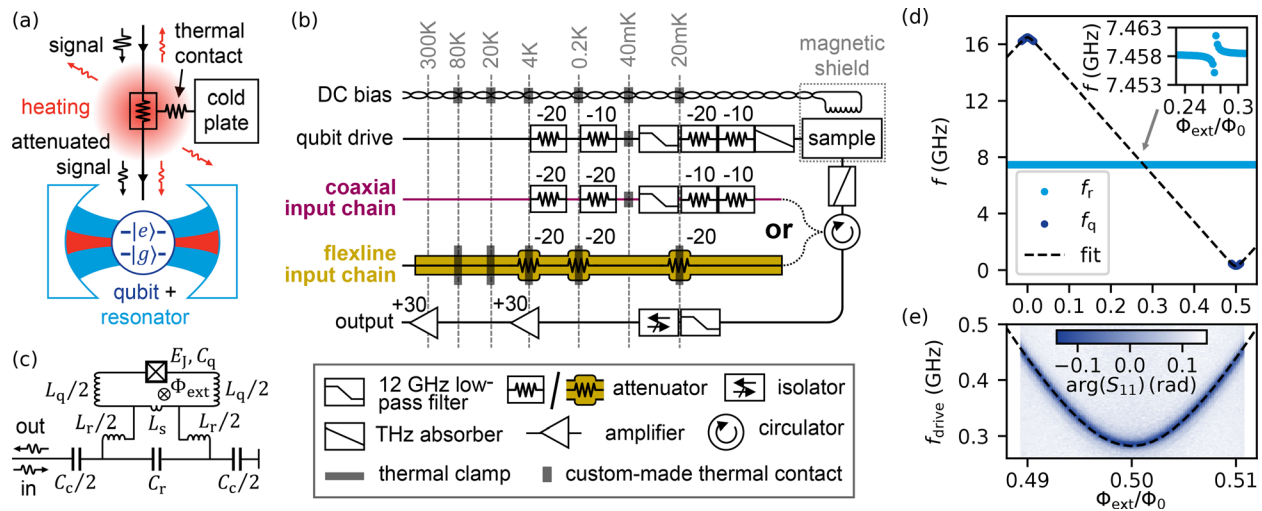


FIG. 1. Cryogenic microwave setup and resonator–qubit device. (a) Principle of measuring the thermalization of input chains. Microwave power dissipated in the attenuators generates local heating which radiates toward the resonator–qubit device, deteriorating its performance. (b) Microwave setup with a direct current (DC) line for magnetic flux biasing of the fluxonium, and three microwave lines for qubit control as well as readout signal input and output. The input chain is implemented either as a coaxial cable with SubMiniature A (SMA) connectorized attenuators or a flexible coplanar stripline (“flexline”) with integrated attenuators (model *Crioflex*[®] 3, see Ref. 26). Both readout assemblies contain a total of 60 dB attenuation, distributed at various temperature stages. The coaxial attenuators at 20 mK were additionally thermalized via a copper braid (see the supplementary material). The flexline is thermalized to the 40 mK intermediate stage using Ag-plated Cu wires and contains a 12 GHz low-pass filter anchored at 20 mK. To thermalize the flexline, we use custom-designed thermal clamps at 80 K, 20 K, 4 K, 200 mK, and 20 mK, as detailed in the supplementary material. In the output chain, signals are amplified by 60 dB using a high-electron-mobility transistor (HEMT) at 4 K and a room-temperature amplifier. The sample is surrounded by an aluminum and mu-metal shield, as used in Ref. 27. (c) Simplified electrical circuit diagram of the fluxonium with inductance $L'_q = L_q + L_s$, capacitance C_q , Josephson energy E_J , and external flux bias Φ_{ext} . The qubit is coupled inductively to a readout resonator with fundamental mode frequency f_r . The readout resonator is coupled via the capacitance C_c to the microwave lines. (d) Measured resonator and qubit frequencies $f_{r,q}$ as a function of the external flux Φ_{ext} . From the fit (dashed line), we extract the qubit parameters (see Table I). The inset highlights the avoided level crossing between the qubit and resonator modes. (e) Two tone spectroscopy of the qubit around $\Phi_{\text{ext}}/\Phi_0 \approx 0.5$.

regime, the residual \bar{n} is observed to be between 2×10^{-4} and 2×10^{-1} ,^{39–47} orders of magnitude larger than the expected $\sim 10^{-8}$ when in thermal equilibrium at 20 mK. While the lower observed limit corresponds to dephasing rates that are on the edge of measurability with state-of-the-art superconducting qubits,⁴⁰ coherence times are usually dominated by photon shot noise in the upper limit. It is thus crucial to ensure that new microwave input chains do not degrade qubit performance by causing excessive photon shot noise-induced dephasing.

Here, we exploit photon shot noise to quantify the thermalization of different microwave input chains. In addition to the passive heat load from higher temperature stages, the attenuators in the input chain are also heated by readout and control pulses. This active heat load generates additional photon shot noise-induced dephasing,^{39,40} which we use to quantify the thermal contact between the attenuator and the cold plate. In separate cooldowns of our dilution refrigerator (model *Sionludi XL*, see Ref. 48), we compare the performance of two microwave input chains, a conventional coaxial cable and a flexible stripline [Fig. 1(b)]. The microwave setup following the input chains remains unchanged in both cases. Furthermore, we use a separate drive line for qubit manipulation and a DC line for magnetic flux biasing.

In order to assess information about photon shot noise, we use a superconducting quantum circuit consisting of a fluxonium qubit, inductively coupled to a resonator [Fig. 1(c)], implementing the dispersive readout scheme. As described in the supplementary material, we fit the qubit state-dependent response of the readout resonator to extract the resonator linewidth $\kappa/2\pi$ and the dispersive shift $\chi/2\pi$,

i.e., the resonator frequency difference for the qubit in the ground or excited state. The qubit spectrum is depicted in Fig. 1(d), while a close-up around its first-order flux-insensitive point $\Phi_{\text{ext}}/\Phi_0 = 0.5$ is shown in Fig. 1(e). Here, Φ_{ext} denotes the external magnetic flux threading the fluxonium loop and Φ_0 is the magnetic flux quantum. Relevant parameters of the resonator–qubit system are summarized in Table I.

To infer the photon shot noise due to passive heat load in the flexline setup, we perform energy relaxation, Ramsey and echo measurements over a course of 12 h in an interleaved manner [Fig. 2(a)]. The measured energy relaxation rates Γ_1 and decoherence rates $\Gamma_2^{*/\text{echo}}$ fluctuate within 2% and the qubit frequency, extracted from the Ramsey fringes, is stable within a few kHz [Fig. 2(b)]. We estimate photon shot noise-induced dephasing rates $\Gamma_{\bar{n}} \approx \Gamma_{\phi} = \Gamma_2 - \Gamma_1/2$ by using $\Gamma_2 = \Gamma_2^{\text{echo}}$ to extract the fast components of the phase noise that can be associated with the photon shot noise. This results in $\Gamma_{\bar{n}}/2\pi = (2.7 \pm 1.1)$ kHz, which we convert into residual photon numbers $\bar{n} = (2.2 \pm 0.9) \times 10^{-3}$, which is in the lower range of what is commonly observed in the community.^{39–47} For this, we follow the derivation in Refs. 49 and 44 that connects photon shot noise-induced

TABLE I. Parameters of the resonator–qubit device.

f_r (GHz)	$\kappa/2\pi$ (MHz)	$\chi/2\pi$ (MHz)	L'_q (nH)	C_q (fF)	E_J (GHz)
7.458	4.10	−2.70	176	5.73	16.6

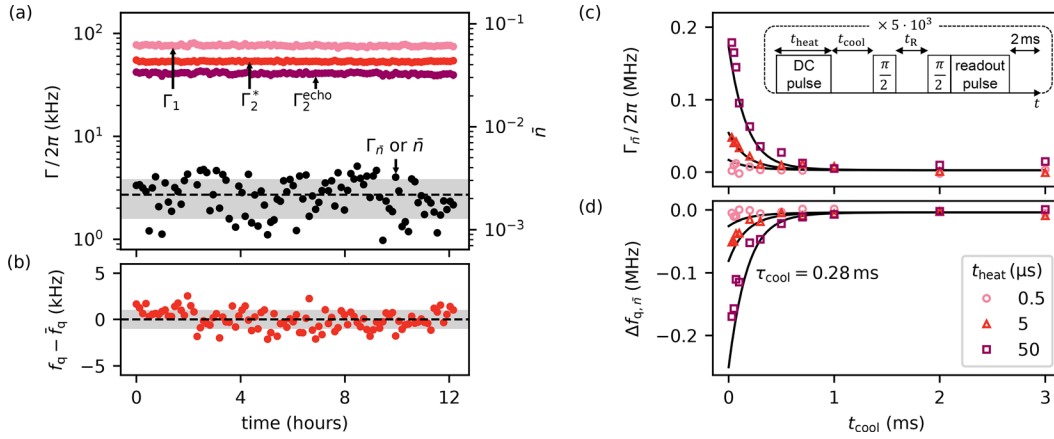


FIG. 2. Fluxonium qubit measurements using the flexible stripline readout at $\Phi_{\text{ext}}/\Phi_0 = 0.5$. (a) Interleaved measurements of Γ_1 relaxation (pink), Γ_2 Ramsey (red), and echo (magenta) dephasing rates over 12 h. Gaussian distribution fits yield values of $\Gamma_1/2\pi = (76.0 \pm 1.4)$ kHz, $\Gamma_2^*/2\pi = (53.3 \pm 0.6)$ kHz, and $\Gamma_2^{\text{echo}}/2\pi = (40.7 \pm 0.9)$ kHz, respectively. Photon shot noise-induced dephasing rates $\Gamma_{\bar{n}}$ (black) are calculated from the extracted Γ_1 and Γ_2^{echo} values as described in the main text and converted into resonator photon numbers \bar{n} according to (2). The dashed line indicates the mean value of $\Gamma_{\bar{n}}$ or \bar{n} and the horizontally filled area their $\pm 1\sigma$ range, as stated in the main text. (b) Qubit frequency extracted from Ramsey fringes fluctuates within a standard deviation of 1.0 kHz around the average qubit frequency \bar{f}_q . (c) The inset shows the pulse sequence for the measurement of attenuator thermalization time. We send a DC pulse of duration t_{heat} in the readout line to heat the attenuators, followed by a variable wait time t_{cool} before a standard Ramsey sequence. The markers correspond to photon shot noise-induced dephasing rates $\Gamma_{\bar{n}}$ as well as (d) qubit frequency shifts $\Delta f_{q,\bar{n}}$ extracted from Ramsey measurements. The black lines show a fit with common temperature relaxation time $\tau_{\text{cool}} = 0.28$ ms for all heat pulses, following Eqs. (1) and (3).

dephasing $\Gamma_{\bar{n}}$ and an AC Stark shift Δf_q of the qubit with the average photon population \bar{n} in the resonator,

$$\Gamma_{\bar{n}} + 2\pi i \Delta f_q = \frac{\kappa}{2} \left(\sqrt{\left(1 + \frac{i\chi}{\kappa}\right)^2 + \frac{4i\chi}{\kappa} \bar{n} - 1} \right). \quad (1)$$

The frequency shift $\Delta f_q = \Delta f_{q,\bar{n}} + \Delta f_{q,0}$ consists of a photon number-dependent term $\Delta f_{q,\bar{n}}$ and the Lamb shift $\Delta f_{q,0} = (\chi/2\pi)/2$. In the regime of $|\chi| \lesssim \kappa$, we can write the following in the limit of small photon numbers $\bar{n} \leq 0.1$:

$$\Gamma_{\bar{n}} + 2\pi i \Delta f_{q,\bar{n}} = \frac{\kappa\chi}{\kappa^2 + \chi^2} (\chi + i\kappa)\bar{n}. \quad (2)$$

In order to evaluate the thermalization of the flexible stripline, we implement the pulse sequence illustrated in Fig. 2(c). Before each repetition, we couple a DC pulse into the input chain with a combiner to actively heat the attenuators. This heat pulse has a power of 4 dBm before entering the cryostat, corresponding to a heat input of 0.25 μW on the dilution stage attenuator and orders of magnitude larger in amplitude than what is used for the readout pulse. We then wait a variable time t_{cool} before performing a Ramsey sequence, from which we can infer the excess photon shot noise and the temperature of attenuators. After each repetition, we wait 2 ms to prevent cumulative heating. To extract $\Gamma_{\bar{n}}$, we subtract from all measured decoherence rates Γ_2^* the same offset value such that, for large t_{cool} , $\Gamma_{\bar{n}}$ corresponds to the average value found in Fig. 2(a). Extracted values for $\Gamma_{\bar{n}}$ and $\Delta f_{q,\bar{n}}$ as a function of t_{cool} are depicted in Figs. 2(c) and 2(d) for three heat pulse durations, $t_{\text{heat}} \in [0.5, 5, 50] \mu\text{s}$.

We model the data using Eq. (1), assuming the input chain is a blackbody radiator with effective temperature T and Bose-Einstein distribution $n_{\text{BE}}(T)$. We associate the temperature-dependent photon

number $\bar{n}(T) = n_{\text{BE}}(f_r, T)$ with the blackbody radiation at frequency $f = f_r$. This temperature rises from its thermal equilibrium T_{eq} by ΔT and relaxes exponentially with a time constant τ_{cool} after the heat pulse,

$$\bar{n}(t_{\text{cool}}) = \left(\exp\left(\frac{hf_r}{k_B T(t_{\text{cool}})}\right) - 1 \right)^{-1} \quad \text{with} \quad (3)$$

$$T(t_{\text{cool}}) = T_{\text{eq}} + \Delta T \exp\left(-\frac{t_{\text{cool}}}{\tau_{\text{cool}}}\right),$$

where k_B and h are the Boltzmann and the Planck constants, respectively.

After a heating pulse, the thermalization of the flexible stripline temperature is modeled by a simultaneous fit of the measured relaxation curves $\Gamma_{\bar{n}}$ and $\Delta f_{q,\bar{n}}$ to Eqs. (1) and (3), yielding a common time constant $\tau_{\text{cool}} = 0.28$ ms for all three values of t_{heat} [Figs. 2(c) and 2(d)]. In Eq. (3), we fix the equilibrium temperature $T_{\text{eq}} = 58$ mK of the blackbody, corresponding to the mean residual thermal photon population in Fig. 2(a). The fit yields temperature differences $\Delta T = [24, 55, 114]$ mK. As shown in the supplementary material, we repeated the same experiment for the coaxial cable setup, resulting in a time constant of $\tau_{\text{cool}} = 0.55$ ms. This indicates that the flexible stripline integrated attenuators are at least as well thermalized as the coaxial cable attenuators.

Even though the model in Eq. (3) fits the data, this is only a first-order approximation. While all attenuators in our setups are thermalized to temperatures $T < 10$ K, in which case both heat capacity and conduction in metals are dominated by electrons,⁵⁰ so thermalization is independent of temperature, this model ignores two factors. First, the non-linear relationship between T and \bar{n} implies that even attenuators that thermalize with the same rate will contribute with different

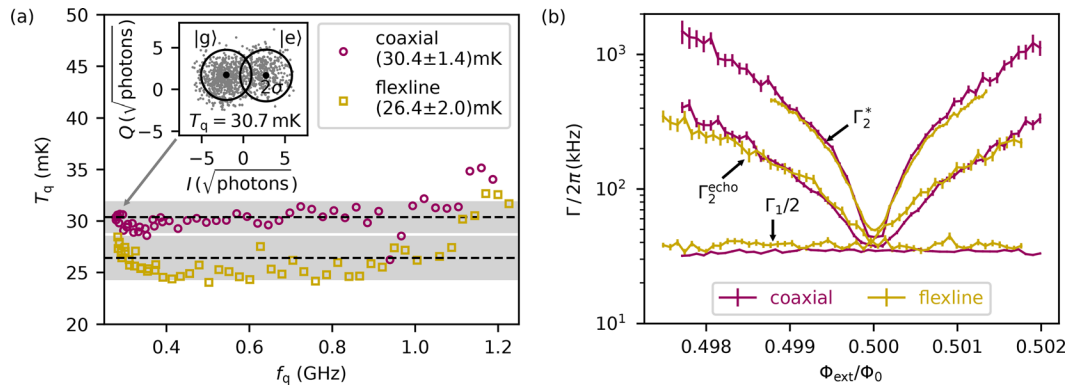


FIG. 3. Comparison of conventional coaxial cable (magenta) and flexible stripline (yellow) setups. (a) Temperature T_q as a function of the qubit frequency f_q , extracted from Gaussian mixture fits of measured IQ distributions. We fit 10^5 points for the coaxial cable and 5×10^4 for the flexible stripline. The dashed lines indicate the mean temperature values \bar{T}_q and the horizontally filled areas the $\pm 1\sigma$ range, as stated in the legend. The inset shows a measured IQ distribution using the coaxial line setup at $\Phi_{\text{ext}}/\Phi_0 = 0.5$, as indicated by the arrow. For better visibility, only a subset of 2000 points is shown. The quadratures are normalized to the square-root of the number of measurement photons $n_{\text{meas}} \approx \bar{n} \kappa t_{\text{meas}}/4$, approximated for negligible internal resonator losses, where \bar{n} is the average number of photons in the resonator and t_{meas} the duration of the readout pulse. The black circles indicate the 2σ regions centered on the pointer states (black markers) corresponding to the qubit in the ground state $|g\rangle$ and the excited state $|e\rangle$, as indicated by the labels. (b) Rates (with vertical errorbars from the fit) extracted from energy relaxation, Ramsey as well as echo experiments in the vicinity of $\Phi_{\text{ext}}/\Phi_0 = 0.5$, for both the coaxial cable and the flexible stripline setup.

time constants to the photon shot noise decay, depending on their respective temperatures. Second, the hot electron effect^{51,52} and increased Kapitza phonon–phonon boundary resistance⁵³ decrease heat conduction at temperatures below a few hundred millikelvin. At different times along the temperature relaxation curve, the photon shot noise might be dominated by attenuators anchored to different stages of the cryostat. Therefore, the extracted values of T_{eq} and ΔT from the fit of the measured data in Figs. 2(c) and 2(d) should be seen as effective parameters characterizing the entire input chain. Future work should develop a more realistic and complex input chain thermal model, where the contributions of each element in the chain to the total photon shot noise are considered independently.

Further comparative measurements with the two input chains show no significant differences in qubit performance (Fig. 3). This includes an extraction of the qubit temperature T_q from IQ distributions over a range of qubit frequencies $f_q \in [0.285, 1.23]$ GHz, obtained by sweeping Φ_{ext} [Fig. 3(a)]. We find T_q for both setups to be almost constant over the whole range and close to the ≈ 20 mK temperature of the dilution stage: (26.4 \pm 2.0) mK for the flexline setup comparable to (30.4 \pm 1.4) mK for the coaxial cable setup. The minor difference in \bar{T}_q is in the range of commonly observed fluctuations between cooldowns. The uptake in T_q for both setups as the qubit frequency decreases below 0.4 GHz or increases beyond 1 GHz could be explained by the fact that the qubit population approaches either 50% or zero, respectively. In both cases, the extracted temperature becomes susceptible to rare out-of-equilibrium excitations, for example from ionizing radiation⁵⁴ or readout quantum-demolition effects.⁵⁵ Moreover, the dispersive shift for large f_q drops to 1/3 of the value at the lowest f_q , making the readout more challenging. In the literature, typical values for T_q fall in a wide range between 20 and 60 mK.^{47,55–59} Finally, Fig. 3(b) shows that the energy relaxation and decoherence rates of the qubit near $\Phi_{\text{ext}}/\Phi_0 = 0.5$ remain unchanged between the two setups within our measurement accuracy.

In conclusion, when using a flexible stripline assembly to connect a qubit readout input chain from room temperature to the dilution

stage of a cryostat, we observe a residual population of the readout resonator of $(2.2 \pm 0.9) \times 10^{-3}$ photons, a 0.28 ms thermalization time of the flexible stripline attenuators, and an effective qubit temperature of 26.4 mK, close to the temperature of the dilution stage. Furthermore, we observe no significant differences in qubit performance when using flexible striplines or conventional coaxial cables. The heating pulse methodology presented here can serve as a simple health check for other groups to test the thermalization of their input chains. These results encourage the use of flexible striplines in future cryogenic microwave setups, enabling at least an order of magnitude increase in the density of microwave input circuitry, paving the way for increasingly complex superconducting detectors and quantum devices.

See the [supplementary material](#) for the following: comparison of the experiments with the coaxial cable setup, similar to the ones shown in Fig. 2, illustration of how the resonator linewidth and the dispersive shift were extracted, presentation of experiments on clamping flexible stripline samples, including a description of the setup, a theoretical model, and a discussion of the measured data, and details on both the flexible stripline as well as the coaxial cable input chain setups.

We are grateful to L. Radtke and S. Diewald for their technical assistance. We thank J. de Groot for support with design and machining as well as D. Rieger and S. Bosman for constructive feedback. We acknowledge funding from the European Commission (FET-Open AVaQus GA 899561). P.P., M.S., and N.G. acknowledge partial funding from the German Ministry of Education and Research (BMBF) within the project GEQCOS (FKZ: 13N15683). V.A. and W. W. acknowledge support from the European Research Council advanced grant MoQuOS (No. 741276). Facilities use was supported by the KIT Nanostructure Service Laboratory (NSL). We thank qKit for providing a convenient measurement software framework.

AUTHOR DECLARATIONS

Conflict of Interest

The authors have no conflicts to disclose.

Author Contributions

Patrick Paluch: Conceptualization (equal); Data curation (equal); Formal analysis (equal); Investigation (equal); Methodology (equal); Resources (equal); Software (equal); Validation (equal); Visualization (equal); Writing – original draft (equal); Writing – review & editing (equal). **Martin Spiecker:** Conceptualization (equal); Methodology (equal); Resources (equal); Software (equal); Supervision (equal); Validation (equal); Visualization (equal); Writing – review & editing (equal). **Nicolas Gosling:** Methodology (equal); Resources (equal); Validation (equal); Visualization (equal); Writing – review & editing (equal). **Viktor Adam:** Data curation (equal); Investigation (equal); Methodology (equal); Resources (equal); Validation (equal); Writing – review & editing (equal). **Jakob Kammhuber:** Resources (equal); Writing – review & editing (equal). **Kiefer Vermeulen:** Resources (equal); Writing – review & editing (equal). **Daniël Bouman:** Resources (equal); Writing – review & editing (equal). **Wolfgang Wernsdorfer:** Methodology (equal); Resources (equal); Supervision (equal); Writing – review & editing (equal). **Ioan M. Pop:** Conceptualization (equal); Data curation (equal); Formal analysis (equal); Funding acquisition (equal); Investigation (equal); Methodology (equal); Project administration (equal); Resources (equal); Software (equal); Supervision (equal); Validation (equal); Visualization (equal); Writing – original draft (equal); Writing – review & editing (equal).

DATA AVAILABILITY

The data that support the findings of this study are available from the corresponding author upon reasonable request.

REFERENCES

- ¹Google Quantum AI, “Suppressing quantum errors by scaling a surface code logical qubit,” *Nature* **614**, 676–681 (2023).
- ²M. Dupont, B. Evert, M. J. Hodson *et al.*, “Quantum-enhanced greedy combinatorial optimization solver,” *Sci. Adv.* **9**, eadi0487 (2023).
- ³Y. Kim, A. Eddins, S. Anand *et al.*, “Evidence for the utility of quantum computing before fault tolerance,” *Nature* **618**, 500–505 (2023).
- ⁴S. Krinner, N. Lacroix, A. Remm *et al.*, “Realizing repeated quantum error correction in a distance-three surface code,” *Nature* **605**, 669–674 (2022).
- ⁵Q. Zhu, S. Cao, F. Chen *et al.*, “Quantum computational advantage via 60-qubit 24-cycle random circuit sampling,” *Sci. Bull.* **67**, 240–245 (2022).
- ⁶E. E. Wollman, V. B. Verma, A. E. Lita *et al.*, “Kilopixel array of superconducting nanowire single-photon detectors,” *Opt. Express* **27**, 35279–35289 (2019).
- ⁷A. Catalano, R. Adam, P. A. R. Ade *et al.*, “The NIKA2 Instrument at 30-m IRAM Telescope: Performance and results,” *J. Low Temp. Phys.* **193**, 916–922 (2018).
- ⁸L. Gottardi and K. Nagayashi, “A review of x-ray microcalorimeters based on superconducting transition edge sensors for astrophysics and particle physics,” *Appl. Sci.* **11**, 3793 (2021).
- ⁹L. Gastaldo, K. Blaum, K. Chrysalidis *et al.*, “The electron capture in 163Ho experiment – ECHo,” *Eur. Phys. J. Spec. Top.* **226**, 1623–1694 (2017).
- ¹⁰S. Kempf, M. Wegner, A. Fleischmann *et al.*, “Demonstration of a scalable frequency-domain readout of metallic magnetic calorimeters by means of a microwave SQUID multiplexer,” *AIP Adv.* **7**, 015007 (2017).
- ¹¹B. Dober, Z. Ahmed, K. Arnold *et al.*, “A microwave SQUID multiplexer optimized for bolometric applications,” *Appl. Phys. Lett.* **118**, 062601 (2021).
- ¹²M. Durkin, J. S. Adams, S. R. Bandler *et al.*, “Mitigation of finite bandwidth effects in time-division-multiplexed SQUID readout of TES arrays,” *IEEE Trans. Appl. Supercond.* **31**, 1 (2021).
- ¹³Y. Chen, D. Sank, P. O’Malley *et al.*, “Multiplexed dispersive readout of superconducting phase qubits,” *Appl. Phys. Lett.* **101**, 182601 (2012).
- ¹⁴J. Heinsoo, C. K. Andersen, A. Remm *et al.*, “Rapid high-fidelity multiplexed readout of superconducting qubits,” *Phys. Rev. Appl.* **10**, 034040 (2018).
- ¹⁵S. Krinner, S. Storz, P. Kurpiers *et al.*, “Engineering cryogenic setups for 100-qubit scale superconducting circuit systems,” *EPJ Quantum Technol.* **6**, 1–29 (2019).
- ¹⁶F. Lecocq, F. Quinlan, K. Cicak *et al.*, “Control and readout of a superconducting qubit using a photonic link,” *Nature* **591**, 575–579 (2021).
- ¹⁷A. Youssefi, I. Shomroni, Y. J. Joshi *et al.*, “A cryogenic electro-optic interconnect for superconducting devices,” *Nat. Electron.* **4**, 326–332 (2021).
- ¹⁸M. Shen, J. Xie, Y. Xu *et al.*, “Photonic link from single-flux-quantum circuits to room temperature,” *Nat. Photonics* **18**, 371–378 (2024).
- ¹⁹C. G. Pappas, J. Austermann, J. A. Beall *et al.*, “High-density superconducting cables for advanced ACTPol,” *J. Low Temp. Phys.* **184**, 473–479 (2016).
- ²⁰D. B. Tuckerman, M. C. Hamilton, D. J. Reilly *et al.*, “Flexible superconducting Nb transmission lines on thin film polyimide for quantum computing applications,” *Supercond. Sci. Technol.* **29**, 084007 (2016).
- ²¹A. B. Walter, C. Bockstiegel, B. A. Mazin *et al.*, “Laminated NbTi-on-Kapton microstrip cables for flexible sub-kelvin RF electronics,” *IEEE Trans. Appl. Supercond.* **28**, 1 (2018).
- ²²V. Gupta, B. Yelamanchili, S. Zou *et al.*, “Thin-film Nb/polyimide superconducting stripline flexible cables,” *IEEE Trans. Appl. Supercond.* **29**, 1 (2019).
- ²³S. Zou, B. Yelamanchili, V. Gupta *et al.*, “Low-loss cable-to-cable parallel connection method for thin-film superconducting flexible microwave transmission lines,” *Supercond. Sci. Technol.* **32**, 075006 (2019).
- ²⁴J. P. Smith, B. A. Mazin, A. B. Walter *et al.*, “Flexible coaxial ribbon cable for high-density superconducting microwave device arrays,” *IEEE Trans. Appl. Supercond.* **31**, 1 (2021).
- ²⁵V. Y. Monarkha, S. Simbierowicz, M. Borrelli *et al.*, “Equivalence of flexible stripline and coaxial cables for superconducting qubit control and readout pulses,” *Appl. Phys. Lett.* **124**, 224001 (2024).
- ²⁶Delft Circuits BV, see <https://delft-circuits.com/cri-oflex-technology/core-technology-cryogenic-rf-cable/> for “Cri/oflex® Cryogenic RF Cable Technology,” accessed: November 6, 2024).
- ²⁷L. Grünhaupt, N. Maleeva, S. T. Skacel *et al.*, “Loss mechanisms and quasiparticle dynamics in superconducting microwave resonators made of thin-film granular aluminum,” *Phys. Rev. Lett.* **121**, 117001 (2018).
- ²⁸M. Kjaergaard, M. E. Schwartz, J. Braumüller *et al.*, “Superconducting qubits: Current state of play,” *Annu. Rev. Condens. Matter Phys.* **11**, 369–395 (2020).
- ²⁹A. Somoroff, Q. Ficheux, R. A. Mencia *et al.*, “Millisecond coherence in a superconducting qubit,” *Phys. Rev. Lett.* **130**, 267001 (2023).
- ³⁰M. Bal, A. A. Murthy, S. Zhu *et al.*, “Systematic improvements in transmon qubit coherence enabled by niobium surface encapsulation,” *npj Quantum Inf.* **10**, 1–8 (2024).
- ³¹G. Zimmerli, T. M. Eiles, R. L. Kautz *et al.*, “Noise in the Coulomb blockade electrometer,” *Appl. Phys. Lett.* **61**, 237–239 (1992).
- ³²F. C. Wellstood, C. Urbina, and J. Clarke, “Low-frequency noise in DC superconducting quantum interference devices below 1 K,” *Appl. Phys. Lett.* **50**, 772–774 (1987).
- ³³D. J. Van Harlingen, T. L. Robertson, B. L. T. Plourde *et al.*, “Decoherence in Josephson-junction qubits due to critical-current fluctuations,” *Phys. Rev. B* **70**, 064517 (2004).
- ³⁴A. Blais, A. L. Grimsmo, S. M. Girvin *et al.*, “Circuit quantum electrodynamics,” *Rev. Mod. Phys.* **93**, 025005 (2021).
- ³⁵P. Bertet, I. Chiorescu, G. Burkard *et al.*, “Dephasing of a superconducting qubit induced by photon noise,” *Phys. Rev. Lett.* **95**, 257002 (2005).
- ³⁶D. I. Schuster, A. Wallraff, A. Blais *et al.*, “AC stark shift and dephasing of a superconducting qubit strongly coupled to a cavity field,” *Phys. Rev. Lett.* **94**, 123602 (2005).
- ³⁷J. Gambetta, A. Blais, D. I. Schuster *et al.*, “Qubit-photon interactions in a cavity: Measurement-induced dephasing and number splitting,” *Phys. Rev. A* **74**, 042318 (2006).
- ³⁸A. P. Sears, A. Petrenko, G. Catelani *et al.*, “Photon shot noise dephasing in the strong-dispersive limit of circuit QED,” *Phys. Rev. B* **86**, 180504 (2012).

- ³⁹J.-H. Yeh, J. LeFebvre, S. Premaratne *et al.*, “Microwave attenuators for use with quantum devices below 100 mK,” *J. Appl. Phys.* **121**, 224501 (2017).
- ⁴⁰Z. Wang, S. Shankar, Z. K. Mineev *et al.*, “Cavity attenuators for superconducting qubits,” *Phys. Rev. Appl.* **11**, 014031 (2019).
- ⁴¹F. Yan, S. Gustavsson, A. Kamal *et al.*, “The flux qubit revisited to enhance coherence and reproducibility,” *Nat. Commun.* **7**, 1–9 (2016).
- ⁴²F. Yan, D. Campbell, P. Krantz *et al.*, “Distinguishing coherent and thermal photon noise in a circuit quantum electrodynamical system,” *Phys. Rev. Lett.* **120**, 260504 (2018).
- ⁴³B. Suri, Z. K. Keane, R. Ruskov *et al.*, “Observation of Autler–Townes effect in a dispersively dressed Jaynes–Cummings system,” *New J. Phys.* **15**, 125007 (2013).
- ⁴⁴C. Rigetti, J. M. Gambetta, S. Poletto *et al.*, “Superconducting qubit in a waveguide cavity with a coherence time approaching 0.1 ms,” *Phys. Rev. B* **86**, 100506 (2012).
- ⁴⁵J. Goetz, S. Pogorzalek, F. Deppe *et al.*, “Photon statistics of propagating thermal microwaves,” *Phys. Rev. Lett.* **118**, 103602 (2017).
- ⁴⁶G. Zhang, Y. Liu, J. J. Raftery *et al.*, “Suppression of photon shot noise dephasing in a tunable coupling superconducting qubit,” *npj Quantum Inf.* **3**, 1–4 (2017).
- ⁴⁷D. Rieger, S. Günzler, M. Spiecker *et al.*, “Granular aluminium nanojunction fluxonium qubit,” *Nat. Mater.* **22**, 194–199 (2023).
- ⁴⁸Qinu GmbH, see <https://qinu.de/version-xl/> for “Sionludi XL Table-Top Dilution Cryostats” (accessed: November 6, 2024).
- ⁴⁹A. A. Clerk and D. W. Utami, “Using a qubit to measure photon-number statistics of a driven thermal oscillator,” *Phys. Rev. A* **75**, 042302 (2007).
- ⁵⁰F. Pobell, *Matter and Methods at Low Temperatures* (Springer, Berlin, Germany, 1996).
- ⁵¹M. L. Roukes, M. R. Freeman, R. S. Germain *et al.*, “Hot electrons and energy transport in metals at millikelvin temperatures,” *Phys. Rev. Lett.* **55**, 422–425 (1985).
- ⁵²F. C. Wellstood, C. Urbina, and J. Clarke, “Hot-electron effects in metals,” *Phys. Rev. B* **49**, 5942–5955 (1994).
- ⁵³W. A. Little, “The transport of heat between dissimilar solids at low temperatures,” *Can. J. Phys.* **37**, 334 (1959).
- ⁵⁴A. P. Vepsäläinen, A. H. Karamlou, J. L. Orrell *et al.*, “Impact of ionizing radiation on superconducting qubit coherence,” *Nature* **584**, 551–556 (2020).
- ⁵⁵D. Gusenkova, M. Spiecker, R. Gebauer *et al.*, “Quantum nondemolition dispersive readout of a superconducting artificial atom using large photon numbers,” *Phys. Rev. Appl.* **15**, 064030 (2021).
- ⁵⁶M. Spiecker, P. Paluch, N. Gosling *et al.*, “Two-level system hyperpolarization using a quantum Szilard engine,” *Nat. Phys.* **19**, 1320–1325 (2023).
- ⁵⁷U. Vool, I. M. Pop, K. Sliwa *et al.*, “Non-poissonian quantum jumps of a fluxonium qubit due to quasiparticle excitations,” *Phys. Rev. Lett.* **113**, 247001 (2014).
- ⁵⁸B.-L. Najera-Santos, R. Rousseau, K. Gerashchenko *et al.*, “High-sensitivity AC-charge detection with a MHz-frequency fluxonium qubit,” *Phys. Rev. X* **14**, 011007 (2024).
- ⁵⁹X. Y. Jin, A. Kamal, A. P. Sears *et al.*, “Thermal and residual excited-state population in a 3D transmon qubit,” *Phys. Rev. Lett.* **114**, 240501 (2015).